Investigation on Stationarity of V2V Channels in a Highway Scenario

Daniel Czaniera[1], Martin Käske[1], Gerd Sommerkorn[1], Christian Schneider[1],
Reiner S. Thomä[1], Giovanni Del Galdo[1], Mate Boban[2], Jian Luo[2]
[1]Institute for Information Technology, Technische Universität Ilmenau, Ilmenau, Germany
E-mail: daniel.czaniera@tu-ilmenau.de
[2]Huawei Technologies Düsseldorf GmbH, 80992 München, Germany
E-mail: mate.boban@huawei.com

***Abstract*—This contribution investigates the stationarity of the vehicle to vehicle (V2V) channel in terms of distance and time. Due to high inherent mobility, the channel can not be assumed to follow the wide sense stationary (WSS) and uncorrelated scattering (US) assumption. Therefore, new evaluation methods have to be applied. We assess the stationarity for a V2V highway scenario using the generalized local scattering function (GLSF) and its collinearity based on measurements. We compare results for exemplary traffic situations and investigate the influence of the antenna placements on the stationarity of the channel. Our results show a strong relation between the stationarity time and the change and rate-of-change of distance between transmitter and receiver.**

***Index Terms* — V2V, channel sounding, measurement, stationarity, local scattering function, collinearity.**

I. Introduction

Due to the rise of connected automated driving, the characteristics of the vehicle to everything (V2X) and more specifically vehicle to vehicle (V2V) communications channel raised more and more interest over the last decade. Given its significant differences compared to channels in classical cellular networks, mainly in terms of stationarity, the research on this topic comes with a lot of challenges. One example is the extraction of large-scale parameters (LSP) from measurement data. Usually, the measured impulse responses are averaged over a number of snapshots, given that the wide sense stationary (WSS) as well as the uncorrelated scattering (US) assumption holds for the investigated channel (WSSUS channels for short). However, due to its inherent mobility, the V2X channel can not be assumed to be WSSUS. Thus, new methods are necessary to evaluate the channel in terms of parameter extraction. One proposal on this, using the so called generalized local scattering function (GLSF), was made in [1]. Further investigations on this methodology have been made in [2]–[4] and others. Apart from parameter extraction, the stationarity of the channel is of high interest for system design as well. Some investigations have been conducted dealing explicitly with the stationarity time and distance within V2X channels [4]–[7]. This paper aims to provide another step towards a deeper understanding of this topic. We used the GLSF and derived the collinearity (see [3], [4], [6]) to obtain stationarity time and distance intervals. In contrast to previous work, we additionally investigate how the positioning of the antennas at the receiver and transmitter influence these results.

II. Measurement Campaign

The data used in this paper were obtained during a channel sounding measurement campaign that took place in August 2017 on a highway near Ilmenau, Germany. Table I summarizes the set-up of the measurement system. Both the transmitter (Tx) and receiver (Rx) were installed into station wagons, each equipped with five antenna elements, leading to a 5x5 multiple input multiple output (MIMO) configuration. We want to emphasize the placement of the antenna elements (see Fig. 1), which we chose to be close to possible applications. While all elements at the Tx as well as the elements 1,2 and 5 at the Rx car were omni-directional antennas, the elements 3 and 4 at the Rx were patch antennas, integrated into the rear bumper. During the measurements, different maneuvers were executed. Further details are given in Section IV.

To evaluate how the stationarity regions depend on the antenna positioning, we split up the 5x5 MIMO configuration into feasible subsets as shown in Table II. This provides us with varying "view-points" onto the respective scenario.

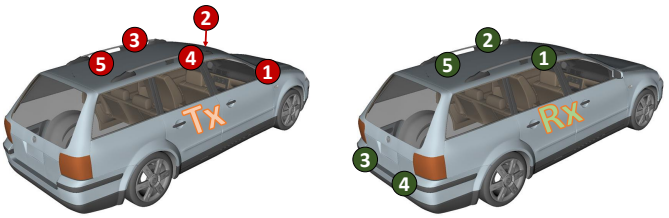

Fig. 1. Schematic of the transmitter and receiver car showing the mounting points of the antenna elements

III. Data Processing

As already stated, the V2X channel is not stationary, as is indicated by an example of a highly time-varying power delay profile (PDP) presented in Fig. 2. It can be seen that the base delay varies rapidly due to changes in Tx-Rx distance. Furthermore, Fig. 2 illustrates that additional components emerge, whose delays do not follow the change of

TABLE I
MEASUREMENT SYSTEM

Channel Sounder	RUSK (MEDAV GmbH)
Transmit signal & power	multi tone @40 dBm
Bandwidth & center frequency	20 MHz @2.53 GHz
Channel impulse response length	6.4 µs
MIMO snapshot rate	2.6 kHz
MIMO sub-channels	5x5 (#Tx x #Rx) w/o guard
Metadata	GPS and 360°-Video

TABLE II
MIMO CONFIGURATIONS

Description	MIMO	Tx Elements	Rx Elements
all links	5x5	1-5	1-5
roof to roof	3x3	3,4,5	1,2,5
roof to rear	3x2	3,4,5	3,4
front to roof	2x3	1,2	1,2,5

the base delay (e.g. starting at around 15 s). Thus, 'classical' approaches in terms of data processing can not be used. In [1] an alternative method was proposed, introducing the GLSF.

A. Generalized Local Scattering Function

A local scattering function can be interpreted as a time-frequency-variant scattering function. To compute the GLSF, local filtering in time and frequency of the measured time-variant transfer function $H(t,f)$ is applied. The extent of these time and frequency extracts must be small enough to assure quasi-stationarity within them. As (1) shows, a 2-D Fourier transform (FT) of these quasi-stationary regions of $H(t,f)$ gives us a time-frequency-variant spreading function.

$$S^{G_k}(t,f;f_D,\tau) = \mathrm{e}^{j2\pi f\tau} \iint H(t',f') \\ G_k^*(t'-t,f'-f)\mathrm{e}^{-j2\pi(f_D\Delta t'-\tau f')}\mathrm{d}t'\mathrm{d}f' \tag{1}$$

The filter function can be expressed as

$$G_k(t,f) = g_i(t)g_j(f), \tag{2}$$

where $g_i(t)$ and $g_j(f)$ are window functions in time and frequency domain. The GLSF is defined as

$$\widetilde{C}_S(t,f;f_D,\tau) = E\left\{\sum_{k=0}^{K-1}\gamma_k|S^{G_k}(t,f;f_D,\tau)|^2\right\}, \tag{3}$$

with $\sum_{k=1}^{K}\gamma_k = 1$ and K being the number of applied filter functions. Fig. 3 shows an example of a GLSF. The resolution in the delay and Doppler domain is slightly worse compared to the spreading function taken directly from the time-varying transfer function $H(t,f)$ due to the application of the aforementioned filter functions.

B. Processing Parameters

To obtain a reliable estimate of the GLSF from small time and frequency intervals, a multitaper approach, using discrete prolate spheroidal sequence (DPSS) [8] as window functions $g_i(t)$ and $g_j(f)$ is proposed [2]. We chose to use two windows in each domain ($I = J = 2$), leading to four 2-D windows in total ($K = 4$), without making any claims on optimality. Using the methods in [2] and [6], we evaluated the minimum quasi-stationary lengths, used as the respective window lengths, as

$$T_{s,min} = \frac{d_{s,min}}{v_{max}} = \frac{1.186\,\mathrm{m}}{60\,\mathrm{m/s}} = 19.8\,\mathrm{ms} \tag{4}$$

$$B_{s,min} = \frac{c_0}{w_{max}} = \frac{3\times10^8\,\mathrm{m/s}}{17\,\mathrm{m}} = 18.75\,\mathrm{MHz} \tag{5}$$

with $d_{s,min}$ being the minimum stationary distance which was set to $10\lambda_c$, v_{max} denoting the maximum relative speed, c_0 being the speed of light in vacuum and w_{max} describing the maximum width of a scatterer being present in the scenario. The latter was set to 17 m, in accordance with the length of a truck.We assumed 18.75 MHz being close enough to the total measured bandwidth of 20 MHz to justify setting the window length in frequency domain to the total bandwidth. Thus, we hereafter omit the dependence of the GLSF on the frequency and name it $\widetilde{C}_S(t;f_D,\tau)$. In time domain, we chose a length of 32 MIMO snapshots, corresponding to a temporal length of 12.3 ms, which is a safe choice in order to not violate the stationarity constraint of the channel.

C. Stationarity Intervals

We obtained the length of the stationarity intervals by inspecting how long the computed GLSF at a given time instance stays 'similar'. Hereby, similarity is measured using the collinearity, which is calculated via

$$col\left\{\widetilde{C}_S\right\}[t_1,t_2] = \frac{tr\left\{\widetilde{C}_S^H(t_1;f_D,\tau)\widetilde{C}_S(t_2;f_D,\tau)\right\}}{\|\widetilde{C}_S(t_1;f_D,\tau)\|_F\|\widetilde{C}_S(t_2;f_D,\tau)\|_F} \tag{6}$$

where $tr\{\dots\}$ is the trace operator and $\|\dots\|_F$ denotes the Frobenius norm. Since the collinearity is based on the GLSF, it takes into account changes in the delay as well as the Doppler domain. On the other hand, due to the normalization factors, the overall power does not affect the outcome. The magnitude of the collinearity ranges from 1 to 0, where 1 indicates identity and values close to 0 denote a great dissimilarity of the compared samples. Thus, the resulting square and symmetric matrix holds values of 1 on the main diagonal. The collinearity can be interpreted as the sum of the element-wise product of two GLSFs. If there is no significant overlap of the two GLSFs in both delay and Doppler domain, the collinearity will give a low value. An exemplary collinearity matrix is presented in Fig. 4. The i'th column of the matrix represents the similarity of the GLSF at the i'th time instance with all other GLSFs, with the i'th element of the i'th column being 1 by definition (similarity of i'th GLSF with itself). We thus expect decreasing values the farther we move away from the i'th element in both directions (i.e. smaller and larger time instances). Applying a threshold of $\epsilon = 0.9$ (as used in [3], [4] and [6]) to the collinearity matrix, we can find the stationarity time T_{stat} for each column (each time instance) as the span of time instances where the collinearity is above the threshold starting from the i'th element of the i'th column – span is

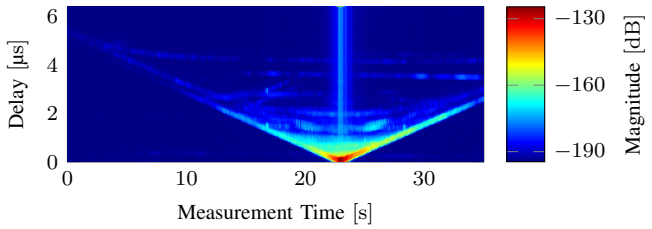

Fig. 2. Example of a strongly time-varying PDP

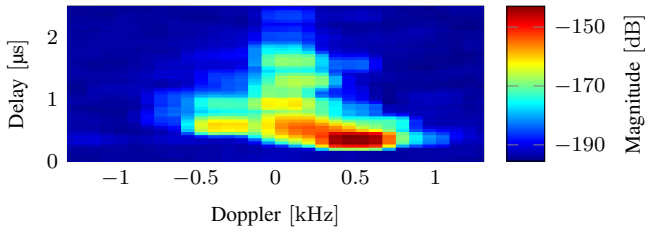

Fig. 3. Example of a GLSF matrix taken from *V2V Highway - Driving in Opposite Direction* measurement at about 7s; averaged over all MIMO links

hereby referring to both larger and smaller time instances (see the black boundaries in Fig. 4). If we further connect the start and the end of the interval to the GPS data, we find a certain distance that the Tx and Rx car traveled within this interval. We refer to this as the stationarity distance d_{stat}.

IV. Results

This section presents exemplary results taken from two highway measurement tracks of the campaign.

A. V2V Highway - Driving in Opposite Direction

The first example recreates a high speed opposite driving scenario. During this measurement, both cars were traveling at roughly $26\,\mathrm{m/s}$ in opposite directions on the highway. To get an idea about the power regime, Fig. 5 shows the peak to noise ratio (PNR) curves (averaged over links and frequencies) for the four MIMO configurations, mentioned in Section II.

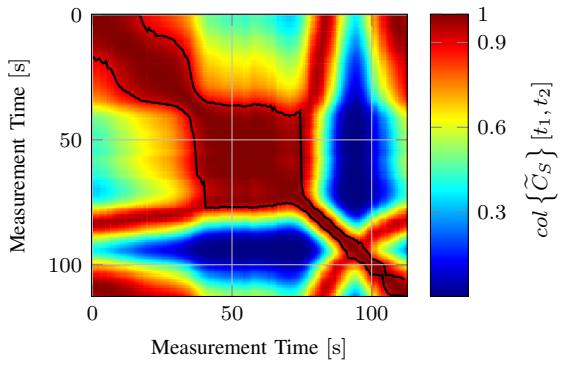

Fig. 4. Collinearity matrix of the *V2V Highway - Driving in Same Direction* measurement track; the black lines show the boundaries of the found stationarity interval

At about $10\,\mathrm{s}$, both cars passed by each other, which results in a peak in the PNR values of all presented configurations. We find that the PNR curves for *all links* and *roof to roof* configurations have a similar trend. In contrast to that, the curves of the *front to roof* and *roof to rear* cases differ greatly. Given by the trajectories of the cars, the front elements at the Tx only face the Rx car until the moment of passing, which leads to a rapid decrease of the PNR in the *front to roof* case after that. The opposite trend of the *roof to rear* configurations PNR is induced by the fact that the rear facing antenna elements at the Rx receive significantly more signal power, after the passing.

Fig. 6 depicts the stationarity time as well as the stationarity distances for the Tx and Rx for the *all links* configuration, respectively. We observe a high correlation between the stationarity time and distance curves, which is the result of the relatively constant speed of both cars throughout the measurement. Due to this, we only provide the stationarity time results for the three remaining configurations in Fig. 7. Besides three drops, the stationarity time remains relatively constant at around $0.4\,\mathrm{s}$. During the interval of $0.4\,\mathrm{s}$, both the transmitter and receiver car traveled approximately $10\,\mathrm{m}$ ($0.4\,\mathrm{m/s}\times 26\,\mathrm{m/s}$) thus reducing the base delay in the impulse response by $20\,\mathrm{m}$. Given the signal bandwidth of $20\,\mathrm{MHz}$, a single delay bin has an equivalent extent of $15\,\mathrm{m} = \frac{c_0}{20\,\mathrm{MHz}}$, that is slightly increased by the use of the windowing function in the GLSF. We can conclude that the stationarity time of $0.4\,\mathrm{s}$ arises from the reduction of base delay and therefore a reduced overlap of the GLSFs especially of the strong line of sight (LoS) component. In terms of the stationarity lengths, the moment of passing induces a strong decrease, up to a minimum of $67.6\,\mathrm{ms}$ and roughly $1.6\,\mathrm{m}$ for the *all links* configuration. This results from the rapid changes in the Doppler domain induced by the LoS component. It shifts from positive values, through $0\,\mathrm{Hz}$ at the moment of passing, to becoming negative. Two more sharp decreases at around $3\,\mathrm{s}$ and $6\,\mathrm{s}$ may be the result of the Tx passing under a bridge and trucks passing by, respectively, which induced new multipath components (MCs) with only a short lifetime.

We furthermore observe strong differences when comparing the three stationarity time curves in Fig. 7. The T_{stat} of the *roof to roof* configuration is similar to the stationarity time in Fig. 6. In contrast to that, the two remaining curves show large differences due to the passing. While the stationarity time for the *roof to rear* MIMO channels is very similar to the *all links* case, from the moment of the passing until the end of the measurement, both curves differ greatly for the measurement time from $0\,\mathrm{s}$ to $10\,\mathrm{s}$. Comparing the stationarity times of the *front to roof* and *all links* configurations, we observe a contrary behavior. These observations indicate that the antenna elements, which are facing each other, dominate the stationarity of the channel.

To gain an insight into the statistics of the stationarity times, Fig. 8 provides the cumulative distribution functions (CDFs) of all discussed MIMO configurations. We find that *all links* configuration shows the least variance, which is a

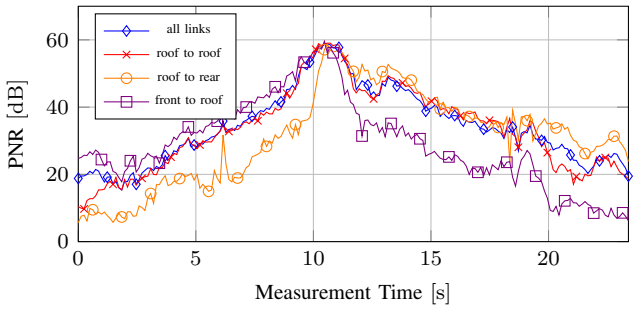

Fig. 5. PNR values of *V2V Highway - Driving in Opposite Direction* for all discussed MIMO configurations

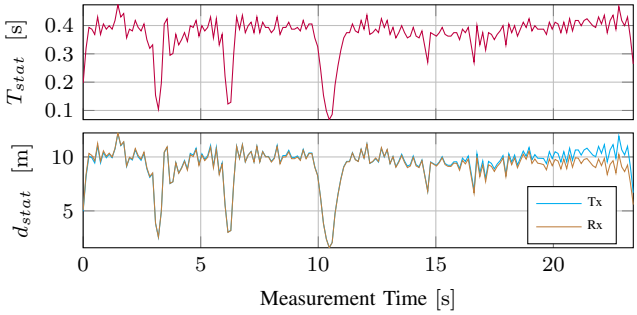

Fig. 6. *V2V Highway - Driving in Opposite Direction* stationarity lengths for *all links*

result of the fact that this configuration resembles a spatial averaging of the channel. Furthermore, this setup holds the overall highest values for the stationarity time, disregarding a few larger values of the *front to roof* configuration. The mean values for all four curves range between $0.34\,\mathrm{s}$ and $0.38\,\mathrm{s}$.

B. V2V Highway - Driving in Same Direction

In contrast to the first example, in this measurement the Tx and Rx vehicle were driving in the same direction. At the beginning, both cars were traveling at roughly $27\,\mathrm{m/s}$, with the Tx directly following the Rx in a convoy scenario. After roughly $55\,\mathrm{s}$, a delivery van, with a height of $2.8\,\mathrm{m}$ and a width of $2\,\mathrm{m}$ was moving in between the two cars. Later on, the Tx accelerated and passed both this van and the Rx vehicle,

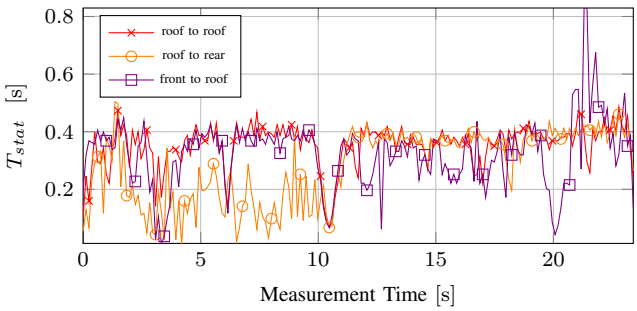

Fig. 7. Stationarity times of *V2V Highway - Driving in Opposite Direction* for the MIMO configurations *roof to roof*, *roof to rear* and *front to roof*

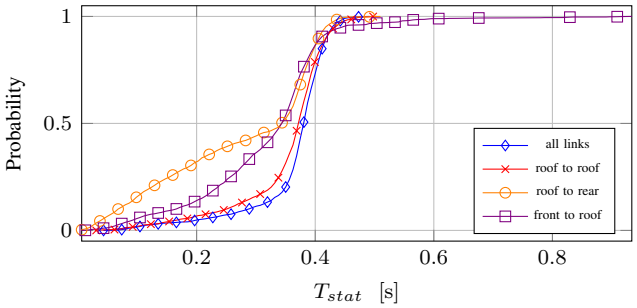

Fig. 8. CDF of the stationarity times of *V2V Highway - Driving in Opposite Direction* for all discussed MIMO configurations

leading to a minimum Tx-Rx distance at around $95\,\mathrm{s}$. The relative velocity of the Tx and Rx as well as their distance is depicted in Fig. 9. The PNR values of all four MIMO configurations only fell below $35\,\mathrm{dB}$ for a few snapshots and were approximately constant during the whole measurement.

Looking at T_{stat} (Fig. 10 and Fig. 11) we find overall higher values compared with the opposite driving scenario. This follows our expectations since the relative velocity between Tx and Rx and therefore the change in base delay and Doppler frequency are much smaller. All stationarity times show three regions during which they undergo only minor changes. The first, ranging from the start of the measurement to roughly $40\,\mathrm{s}$, shows T_{stat} up to $30\,\mathrm{s}$. From Fig. 9 it can be seen that it takes about $30\,\mathrm{s}$ until the distance between Tx and Rx changes by roughly $20\,\mathrm{m}$. This could indicate that the stationarity time is again determined by the change of base delay in the GLSF. The second region ranges from $40\,\mathrm{s}$ to $75\,\mathrm{s}$. During that time period the van is passing the Tx and moves in between both cars. T_{stat} stays at $\approx 40\,\mathrm{s}$ which coincides with the duration of the van being in between the cars. The base delay is not changing during that time. Fig. 11 shows that T_{stat} is much lower for the *roof to rear* configurations indicating that the *rear* antennas of the Rx car are more affected by the van. Furthermore, it can be seen that the stationarity is in general not reduced by the van. That could mean the van was not able to properly block the LoS (except maybe for the *roof to rear* case) or that even with blocked LoS (generating a none line of sight (NLoS) environment) the channel stays stationary. As soon as the Tx is accelerating and passes the van and the Rx (at about $75\,\mathrm{s}$) T_{stat} drops to approximately $4\,\mathrm{s}$. Fig. 9 shows again a connection of this stationarity time with the time it takes to change the Tx-Rx-distance by $20\,\mathrm{m}$. Looking at the different MIMO configurations, we find that the stationarity only varies significantly for the *roof to rear* case. It shows overall lower values and a decrease in the stationarity time to a minimum of $6\,\mathrm{ms}$ after a measurement time of roughly $95\,\mathrm{s}$, i.e. after the passing. The reason may be that the patch antennas in the rear bumper of the receiver car receive no strong (quasi-LoS) signal anymore after the Tx passes the Rx. Fig. 12 provides the CDFs of all discussed MIMO configurations. This diagram shows again the lower values for the *roof to rear* configuration, with a mean value of $21.6\,\mathrm{s}$. All other set-ups differ to a lesser

extent. The stationarity time obtained from the *roof to roof* configuration has the highest average with 27.7 s.

V. Conclusion

We investigated the stationarity distance and time of the V2V channel using channel sounding measurements taken in a highway scenario. From the results we observe a strong relation of the stationarity time with the change in Tx-Rx-distance/base-delay and Doppler frequency in the corresponding GLSFs. We evaluated the influence of the antenna positioning on both the receiving and transmitting car. Our findings indicate in general a larger stationarity time when the respective antennas are mounted on the roof of the cars (as opposed to the bumper or front of the car). We note, that the presented results are specific to the measured scenario. In future work, more diverse traffic situations have to be investigated. We assume that in our examples mostly LoS or quasi-LoS conditions dominated. It can be expected that investigations for NLoS conditions yield different results (e.g. regarding the antenna placement).

Acknowledgment

The authors would like to thank the Thüringer Innovationszentrum Mobilität (ThIMo), the VISTA4F ProExellenz research group funded by the Thüringer Ministerium für Wirtschaft, Wissenschaft und Digitale Gesellschaft as well as the research group "ELVIS" funded by the European Social Fund (ESF) under the grant 2015 FGR 0088. Additionally, we thank Volkswagen AG as well as Fraunhofer IIS for providing the vehicles.

References

[1] G. Matz, "On non-WSSUS wireless fading channels," *IEEE Transactions on Wireless Communications*, vol. 4, no. 5, pp. 2465–2478, Sept 2005.

[2] ——, "Doubly underspread non-WSSUS channels: analysis and estimation of channel statistics," in *2003 4th IEEE Workshop on Signal Processing Advances in Wireless Communications - SPAWC 2003 (IEEE Cat. No.03EX689)*, June 2003, pp. 190–194.

[3] L. Bernado, T. Zemen, A. Paier, J. Karedal, and B. H. Fleury, "Parametrization of the local scattering function estimator for vehicular-to-vehicular channels," in *2009 IEEE 70th Vehicular Technology Conference Fall*, Sept 2009, pp. 1–5.

[4] A. Paier, T. Zemen, L. Bernado, G. Matz, J. Karedal, N. Czink, C. Dumard, F. Tufvesson, A. F. Molisch, and C. F. Mecklenbrauker, "Non-WSSUS vehicular channel characterization in highway and urban scenarios at 5.2GHz using the local scattering function," in *2008 International ITG Workshop on Smart Antennas*, Feb 2008, pp. 9–15.

[5] L. Bernadó, T. Zemen, F. Tufvesson, A. F. Molisch, and C. F. Mecklenbräuker, "The (in-) validity of the WSSUS assumption in vehicular radio channels," in *2012 IEEE 23rd International Symposium on Personal, Indoor and Mobile Radio Communications - (PIMRC)*, Sept 2012, pp. 1757–1762.

[6] A. Ispas, G. Ascheid, C. Schneider, and R. Thoma, "Analysis of local quasi-stationarity regions in an urban macrocell scenario," in *2010 IEEE 71st Vehicular Technology Conference*, May 2010, pp. 1–5.

[7] R. He, O. Renaudin, V. Kolmonen, K. Haneda, Z. Zhong, B. Ai, and C. Oestges, "Characterization of quasi-stationarity regions for vehicle-to-vehicle radio channels," *IEEE Transactions on Antennas and Propagation*, vol. 63, no. 5, pp. 2237–2251, May 2015.

[8] D. Slepian, "Prolate spheroidal wave functions, fourier analysis, and uncertainty - v: The discrete case," *Bell System Technical Journal*, vol. 57, no. 5, pp. 1371–1430, May-June 1978.

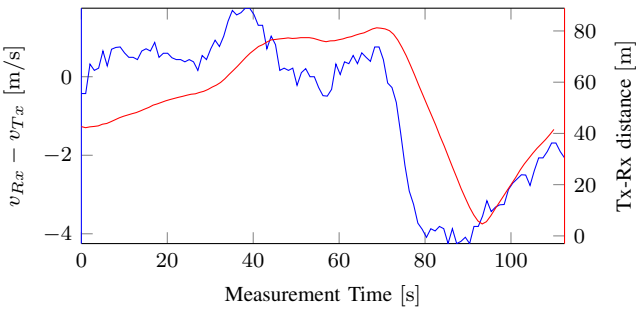

Fig. 9. Relative velocity (blue) and Tx-Rx distance (red) of the *V2V Highway - Driving in Same Direction* measurement

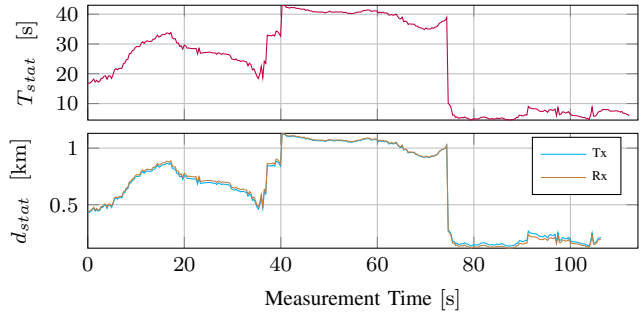

Fig. 10. *V2V Highway - Driving in Same Direction* stationarity lengths for *all links*

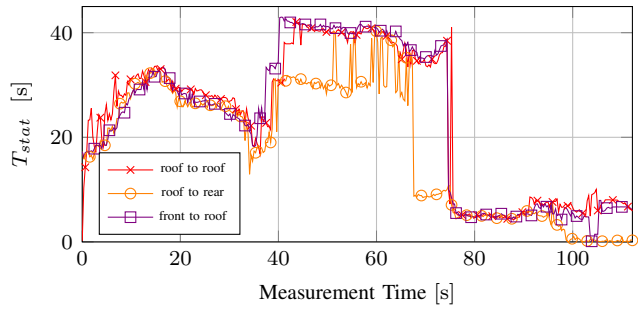

Fig. 11. Stationarity times of *V2V Highway - Driving in Same Direction* for the MIMO configurations *roof to roof*, *roof to rear* and *front to roof*

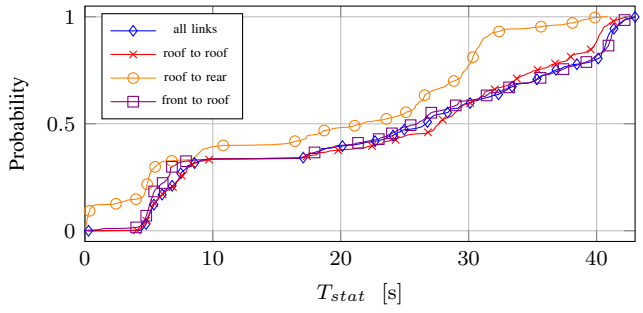

Fig. 12. CDF of the stationarity times of *V2V Highway - Driving in Same Direction* for all discussed MIMO configurations